HTML ABSTRACT + LINKS

Ab initio potential energy surfaces, total absorption cross sections, and product quantum state distributions for the low-lying electronic states of N_2O

Mohammad Noh Daud[a)]
School of Chemistry, University of Bristol, Bristol BS8 1TS, United Kingdom

Gabriel G. Balint-Kurti[b)]
School of Chemistry, University of Bristol, Bristol BS8 1TS, United Kingdom

Alex Brown[c)]
Department of Chemistry, University of Alberta, Edmonton, Alberta T6G 2G2, Canada

(Received 1 September 2004; accepted 20 October 2004; published online 18 January 2005)

Adiabatic potential energy surfaces for the six lowest singlet electronic states of N_2O ($X\,^1A'$, $2\,^1A'$, $3\,^1A'$, $1\,^1A''$, $2\,^1A''$ and $3\,^1A''$) have been computed using an *ab initio* multireference configuration interaction (MRCI) method and a large orbital basis set (aug-cc-pVQZ). The potential energy surfaces display several symmetry related and some nonsymmetry related conical intersections. Total photodissociation cross sections and product rotational state distributions have been calculated for the first ultraviolet absorption band of the system using the adiabatic *ab initio* potential energy and transition dipole moment surfaces corresponding to the lowest three excited electronic states. In the Franck–Condon region the potential energy curves corresponding to these three states lie very close in energy and they all contribute to the absorption cross section in the first ultraviolet band. The total angular momentum is treated correctly in both the initial and final states. The total photodissociation spectra and product rotational distributions are determined for N_2O initially in its ground vibrational state (0,0,0) and in the vibrationally excited (0,1,0) (bending) state. The resulting total absorption spectra are in good quantitative agreement with the experimental results over the region of the first ultraviolet absorption band, from 150 to 220 nm. All of the lowest three electronically excited states [$^1\Sigma^-(1\,^1A'')$, $^1\Delta(2\,^1A')$, and $^1\Delta(2\,^1A'')$] have zero transition dipole moments from the ground state [$^1\Sigma^+(1\,^1A')$] in its equilibrium linear configuration. The absorption becomes possible only through the bending motion of the molecule. The $^1\Delta(2\,^1A') \leftarrow X\,^1\Sigma^+(^1A')$ absorption dominates the absorption cross section with absorption to the other two electronic states contributing to the shape and diffuse structure of the band. It is suggested that absorption to the bound $^1\Delta(2\,^1A'')$ state makes an important contribution to the experimentally observed diffuse structure in the first ultraviolet absorption band. The predicted product rotational quantum state distribution at 203 nm agrees well with experimental observations. © *2005 American Institute of Physics.* [DOI: 10.1063/1.1830436]

I. INTRODUCTION

Nitrous oxide (N_2O) is an important constituent of the atmosphere[1] and is responsible for 5% of the human induced greenhouse effect.[2] In the upper atmosphere, its photodissociation leads to the production of highly reactive oxygen atoms in their first excited electronic state, $O(^1D)$. Since, in the photodissociation process, $O(^1D)$ comprises the major oxygen dissociation channel and its photofragmentation partner, N_2, is chemically inert, the photodissociation of N_2O is often used as a source of $O(^1D)$ atoms for reaction dynamics and kinetics experiments in the laboratory.[3–5]

Leifson[6] first observed and identified the long wavelength N_2O absorption spectrum (150–230 nm) in 1926. Since that time the photoabsorption and subsequent photodissociation of N_2O has received a great deal of experimental,[7–22] and theoretical[12,23–32] interest. The ultraviolet absorption spectrum of N_2O consists of a very broad peak running from about 150 to 220 nm with a maximum near 180 nm and having some superimposed diffuse structure.[7–10,33] In this wavelength region, the photodissociation process

$$N_2O(X\,^1A',v,J)+h\nu \rightarrow N_2(X\,^1\Sigma_g^+,v,j)+O(^1D), \quad (1)$$

which produces nitrogen in its ground electronic state, $N_2(X\,^1\Sigma_g^+)$, and electronically excited state oxygen, $O(^1D)$, dominates. More detailed dynamics experiments[12–20] have been carried out in the long wavelength tail, i.e., at wavelengths of 193, 203, or 205 nm, to measure the energetics and spatial distributions of the photofragments. The experiments have shown that the N_2 produced is highly rotationally excited, mainly vibrationally cold, and that the average an-

a)Electronic mail: M.N.Daud@Bristol.ac.uk
b)Author to whom correspondence should be addressed. Electronic mail: Gabriel.Balint-Kurti@Bristol.ac.uk
c)Electronic mail: alex.brown@ualberta.ca

 © 2005 American Institute of Physics

Downloaded 19 Jan 2005 to 129.128.168.123. Redistribution subject to AIP license or copyright, see http://jcp.aip.org/jcp/copyright.jsp

isotropy parameter β is ≈ 0.5. While there has been consensus on some details of the photodissociation process, the interpretation of the experiments has lead to some conflicting conclusions. We are therefore interested in performing exact quantum mechanical dynamics calculations of the photodissociation process based on *ab initio* potential energy and transition dipole moment surfaces so as to investigate the detailed dynamics underlying the observed photofragmentation processes. We aim here to determine the total absorption cross section as well as the rotational distribution of the resulting N_2 fragments for the photodissociation process.

Experiments at 193 and 203 nm[14,18] have shown that, at these excitation wavelengths, the N_2 products are produced vibrationally cold, with the amount of N_2 in the first excited vibrational state, $v=1$, being less than 2% of that in the ground vibrational state ($v=0$). The lack of vibrational excitation can, most likely, be attributed to the fact that the N_2 bond distance contracts less than 3% from 2.131 99 bohrs in N_2O to 2.074 16 bohrs in N_2 following photodissociation. Hence, the dynamical calculations will be based on two-dimensional potential energy and transition dipole moment surfaces where the N_2 bond length is fixed at 2.131 99 bohrs.

The photodissociation of N_2O represents a very rich dynamical process as underscored by the experiments[12–22] that have been carried out probing both the N_2 and $O(^1D)$ fragments. Both nonstate-selected[14,17] and initial state-selected[12] experiments have shown that the N_2 photofragment is produced rotationally hot, with maximum population in $j=74$. Qualitatively, the rotational excitation can be understood from the strong anisotropy of the excited state surfaces,[12,25,26] $2\,^1A'$ and $1\,^1A''$, which could be involved in the photodissociation process. Neyer *et al.*[14] have determined the J-dependent spatial anisotropy β for the N_2 fragment and have shown that while β is positive for all rotational states ($J=40-90$), the anisotropy decreases with increasing rotational state (confirmed by Janssen and co-workers[12]). The electronic structure calculations of Brown *et al.*[26] and Janssen and co-workers[12] suggest that the transition is dominated by the parallel transition $2\,^1A' \leftarrow X\,^1A'$. The experiments of Ahmed *et al.*[13] on the orbital alignment of the $O(^1D_2)$ fragment have been interpreted to indicate both strong initial parallel and perpendicular excitation. Also, Suzuki *et al.*[16] measure a bimodal recoil distribution of $O(^1D_2)$ atoms providing evidence for two excited states being involved in the dissociation process. The experiments of Suzuki and co-workers can be interpreted as evidence for nonadiabatic transitions between the excited $2\,^1A'$ state and the ground $X\,^1A'$ state but the study of Teule[12] suggests that the dissociation primarily proceeds adiabatically. There is therefore a clear need for quantitative dynamical calculations to help interpret the multitude of detailed, and often conflicting, measurements of the N_2O photodissociation process.

The role of photodissociation in the isotopic enrichment of atmospheric N_2O has also been widely studied.[23,24] The paper of Nanbu and Johnson,[34] which appeared during the writing of this paper, presents a new potential energy surface and also performs time-dependent wave packet calculations of the absorption cross sections. We will compare their conclusions with our own in results and conclusions sections below.

In this paper, we present potential energy surface and transition dipole moment calculations for the lowest six electronic states of N_2O. The calculations are performed at the multireference configuration interaction (MRCI) level of theory and utilize a larger orbital basis set than any so far published. We found this to be necessary because the transition dipole moments are zero to all of the first three excited electronic states at the equilibrium configuration[26] and the absorption cross sections therefore display a great sensitivity of the detailed form of the transition dipole moment surfaces. Also presented are the results of time-dependent wave packet calculations of the photodissociation cross sections for the three lowest excited state and rotational quantum state distributions.

There have been relatively few previous *ab initio* calculations of the singlet excited state potentials of N_2O.[12,25,26] While these potential energy and transition dipole moment surfaces are sufficiently accurate to provide a satisfactory qualitative description of the photodissociation dynamics,[27] they were not sufficiently accurate to provide a quantitative description. Absorption cross sections calculated using these surfaces have been scaled[23] in order to improve the agreement with experimental results. The present work was undertaken so as to achieve an improved agreement between the totally *ab initio* computed cross sections and experiment. It is clear that only through such a reliable theoretical approach will it eventually be possible to fully understand the complex dynamics underlying the detailed and copious experimental results which have now been reported for the N_2O photodissociation process.

The paper is organized as follows: Sec. II gives an overview of the theory, the results are presented in Sec. III and the final section consists of a brief summary of the work.

II. THEORY

A. Potential energy surface calculations

The *ab initio* calculations of the potential energy and transition dipole moment surfaces were performed using the MOLPRO computer code.[35] The calculations for each nuclear geometry on the potential energy surface proceeded by first performing a state averaged complete active space self consistent field (CASSCF) calculation.[36,37] These calculations yielded a set of molecular orbitals and multideterminental or multiconfigurational wave functions which were then used in a multiconfiguration reference internally contracted configuration interaction (MRCI) calculation.[38,39] Many initial tests were performed to determine the best orbital basis set for the calculations. We eventually decided on using the augmented correlation consistent polarized valence quadruple ζ (aug-cc-pVQZ or AVQZ) Gaussian basis set of Dunning,[40,41] but without the g symmetry basis functions. We denote this basis by the acronym AVQZ($-g$). For the N_2O calculations this corresponded to 186 contracted Gaussian orbitals or 225 symmetry adapted primitive Gaussian-type functions. The active space in the CASSCF calculations consisted of nine orbitals, corresponding to the three $2p$ orbitals of each of the

Downloaded 19 Jan 2005 to 129.128.168.123. Redistribution subject to AIP license or copyright, see http://jcp.aip.org/jcp/copyright.jsp

atoms. While a limited number of calculations for collinear geometries were performed using C_{2v} symmetry, most were of, necessity, performed using the C_s symmetry point group, which has just two irreducible representations corresponding to wave functions that are either even (A') or odd (A'') with respect to reflection in the molecular plane. The MRCI calculations used 4 327 880 or 4 121 517 contracted molecular orbital configurations for the A' and A'' calculations, respectively.

B. Quantum calculation of photodissociation cross sections and product state distributions

The first part of a photodissociation calculation is the calculation of the initial bound state wave functions. In order to perform the bound state and photodissociation calculations we must compute the ground and excited state potentials on a grid which is much finer than that used in the *ab initio* calculations. This finer grid is calculated using a two-dimensional cubic spline interpolation procedure.[42,43] The calculations use Jacobi coordinates.[44–46] The coordinates consist of the vector **r** joining the two nitrogen atoms, the vector **R** connecting the center of mass of the nitrogen to the oxygen atom, and the angle θ between these two vectors (zero for linear N–N–O geometry). The wave function is represented on a uniform grid of points in the radial coordinates[47] and on a Gauss–Legendre quadrature grid in the angular coordinate.[48–51] We have recently used similar methods and computer codes to compute the lowest 100 vibrational states of the two lowest electronic states of C_3.[52] These calculations, which report excellent agreement with the experimental results, provide evidence of the reliability of our computer codes.

Time-dependent quantum wave packet calculations were used to compute the total absorption cross section and the product quantum state distributions reported below. The theory of these calculations has been described[42] and reviewed elsewhere.[44,45,53] The absorbed photon can add one unit of angular momentum to the initial wave function of the molecule and the details of treating the coupling of all the angular momenta involved form an important aspect of the theory.[42] As the equilibrium geometry of the parent molecule is linear, the initial wave function may also possess vibrational angular momentum arising from the degenerate bending motion. All of these angular momentum contributions are correctly accounted for in the theory.[42,52] Note in particular that the bound state vibrational wave functions with one quantum of bending vibration have one unit of vibrational angular momentum about the collinear geometry axis and can therefore only exit in a state with a total angular momentum quantum number of at least unity.

As time proceeds the initial wave packet, formed from the product of the initial wave function and the transition dipole moment surface, moves to large values of the radial Jacobi scattering coordinate. As the grid on which the wave packet is represented is of necessity finite, we have to absorb the wave packet near the edge of the grid. We do this using a negative imaginary absorbing potential.[54–56] We use a cubic form of the absorbing potential for this purpose,

TABLE I. Details of grid and other parameters used in the quantum wave packet calculations.

N_2-O dissociation coordinate (R) range (Bohr)	0–14.0
Number of grid points in R	384
Number of angular grid points and basis functions	128[a]
Absorption length (R-R_{damp}) (Bohr)	0.95
Absorption strength (A_{damp}) (a.u.)	0.1014

[a]The N–N exchange symmetry was used, so only 64 angular grid points were required, giving an effective basis set of associated Legendre polynomials of index up to $j=128$.

$$V_{\text{damp}}(R)=\begin{cases} 0.0 & ; \quad R<R_{\text{damp}} \\ -iA_{\text{damp}}\left(\dfrac{R-R_{\text{damp}}}{R_{\text{max}}-R_{\text{damp}}}\right)^3 & ; \quad R_{\text{damp}}\leqslant R\leqslant R_{\text{max}} \end{cases}, \tag{2}$$

where R_{damp} is the point at which the damping is ''switched on'' and A_{damp} is an optimized parameter giving the strength of the damping.

The various grid parameters and the parameters of the damping potential are given in Table I.

III. RESULTS

A. Potential energy and transition dipole moment surfaces

Figure 1 shows a cut through potential energy surfaces of the four lowest singlet electronic states of N_2O in collinear N–N–O geometry with N–N separation fixed at 2.131 99 bohrs. The calculations were performed using C_{2v} symmetry. Separate calculations were performed for the two degenerate components of the $^1\Pi$ [$^1\Pi$ ($1B_1;2A'$) and $^1\Pi$ ($1B_2;1A''$)] and $^1\Delta$ [$^1\Delta$ ($2A_1;2A''$) and $^1\Delta$ ($1A_2;3A'$)] states; where we have noted the symmetries of the electronic states in both collinear, C_{2v} and bent or C_s symmetries. The labels as-

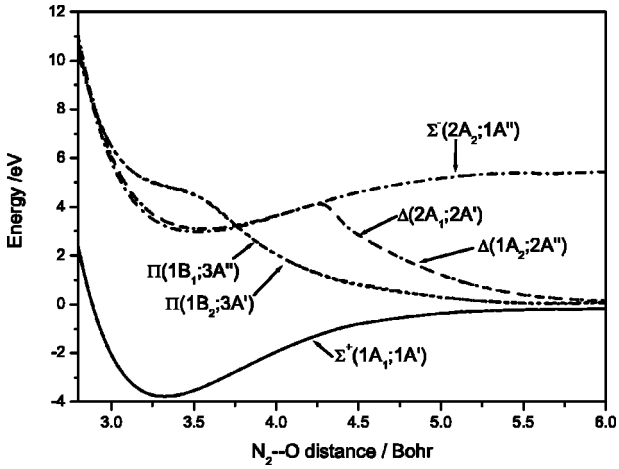

FIG. 1. Cut through potential energy surfaces of the four lowest singlet electronic states of N_2O in collinear N–N–O geometry with N–N separation fixed at 2.131 99 bohrs as a function of the N_2-O distance. The calculations were performed using C_{2v} symmetry. Separate calculations were performed for the two degenerate components of the $^1\Pi$ [$^1\Pi(1B_1)$ and $^1\Pi(1B_2)$] and $^1\Delta$ [$^1\Delta(2A_1)$ and $^1\Delta(1A_2)$] states. The first symmetry notation given in the round brackets is that of the C_{2v} point group, while the second notation is that of the C_s point group which must be used for nonlinear geometries.

Downloaded 19 Jan 2005 to 129.128.168.123. Redistribution subject to AIP license or copyright, see http://jcp.aip.org/jcp/copyright.jsp

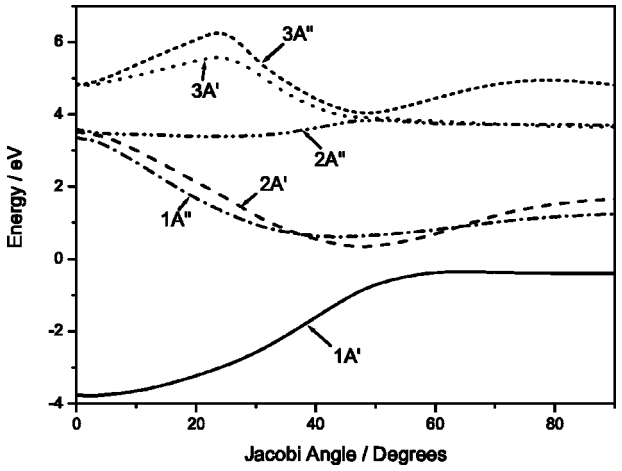

FIG. 2. Cut through potential energy surfaces of the six lowest singlet electronic states of N_2O as the molecule is bent out of the collinear N–N–O geometry with N–N separation fixed at 2.131 99 bohrs and the N_2-O separation fixed at 3.3 bohrs. The calculations were performed using C_s symmetry. The curves correspond to the same electronic states as those shown in Fig. 1.

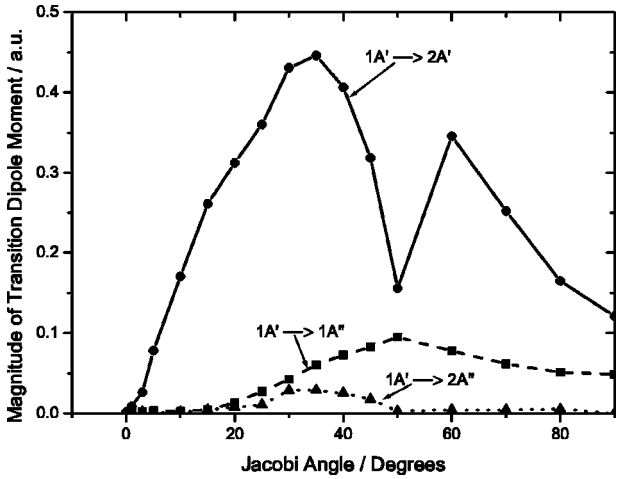

FIG. 3. Magnitude of transition dipole, in atomic units, from the ground state to the three lowest excited states as a function of the Jacobi angle. The N–N separation is fixed at 2.131 99 bohrs and the N_2-O separation at 3.3 bohrs.

signed to the curves in C_s symmetry correspond to their order in the equilibrium geometry of the ground electronic state. The figure immediately shows the presence of four different symmetry related conical intersections where the $^1\Pi$ and $^1\Delta$ curves cross curves of different symmetries in a collinear geometry. There may also be some conical intersections on the inner repulsive wall, where the $^1\Pi$ curves recross the $^1\Sigma^-$ and $^1\Delta$ curves.

Figure 2 shows a cut through the potential energy surfaces of the same electronic states as the molecule is bent away from the collinear geometry with the N_2-O separation fixed at 3.3 bohrs. The ground state has a collinear equilibrium geometry, while the lowest two electronically excited states ($1A''$ and $2A'$) both show a rapid decrease in energy as the molecule is bent. The lowest electronically excited state has $^1\Sigma^-$ symmetry in collinear configuration, while the second and third electronically excited states ($2A'$ and $2A''$) are the degenerate components of the $^1\Delta$ state in collinear geometries. The Renner–Teller coupling between these two states will permit coupling of the wave functions associated with them. As all of the three lowest electronic states lie very close in energy in the collinear Franck–Condon region, this means that, provided there is a nonzero transition dipole moment connecting these states with the ground electronic state, all three states will contribute to the lowest energy UV absorption band of the molecule. In the collinear geometry and in the Franck–Condon region, the transition from the $^1\Sigma^+$ ground electronic state to the $^1\Sigma^-$ and $^1\Delta$ are both dipole forbidden. The transition becomes allowed only through the bending motion of the molecule.

Figure 3 shows the magnitude of the transition dipole connecting the ground state to the three lowest excited states as a function of the bending (Jacobi) angle with the N_2-O separation again being fixed at 3.3 bohrs. It is clear from this figure that the transition to the $2A'$ state will dominate the absorption spectrum. Note that the transition dipole is a vector quantity and that we compute two separate components of the $2A'\leftarrow 1A'$ transition dipole and use them as prescribed by the theory given in Ref. 42. It is the component of the transition dipole which lies in the molecular plane, but is perpendicular to the Jacobi scattering coordinate **R** which gives rise to the "perpendicular" excitation component of the absorption noted by Ahmed *et al.*[13] The sharp dip in the magnitude of the $2A'\leftarrow 1A'$ transition dipole at around 50° coincides with the region of the conical intersection between the two lowest A' states (see Ref. 26 for a more detailed discussion).

Figure 4 shows contour maps of the lowest four potential energy surfaces. The regions of conical intersection in collinear geometries are clearly seen around a N_2-O separation of 3.7 bohrs for the $2A'$ and $1A''$ surfaces and around 4.3 bohrs for the $2A''$ state (see also Fig. 1). The region of another conical intersection cone is also apparent at around 50° and a N_2-O separation of 3.4 bohrs in the $1A'$ ground state [Fig. 4(a)] and the $2A'$ excited state [Fig. (4b)] surfaces (see also Ref. 26). The potential energy and transition dipole moment surfaces used in this work are available through the American Institute of Physics Electronic Physics Auxiliary Publication Service (EPAPS).[57]

B. Photodissociation cross sections and product quantum state distributions

Table II shows the results of our calculated bound states and compares them with the experimentally observed energy levels. We see that our two-dimensional grid based calculations, with the N–N separation held fixed, on the unscaled ground state potential energy surface gives good agreement with the experimental energy levels.

Figure 5 shows the $2A'\leftarrow 1A'$ cross sections calculated using *ab initio* potential energy surfaces and transition dipole moment surfaces computed using different basis sets. We see that there is a dramatic reduction of the computed magnitude of the cross section as the basis set is increased from augmented correlation consistent polarized valence double ζ (AVDZ normally denoted as aug-cc-pVDZ),[40,41] to triple ζ

Downloaded 19 Jan 2005 to 129.128.168.123. Redistribution subject to AIP license or copyright, see http://jcp.aip.org/jcp/copyright.jsp

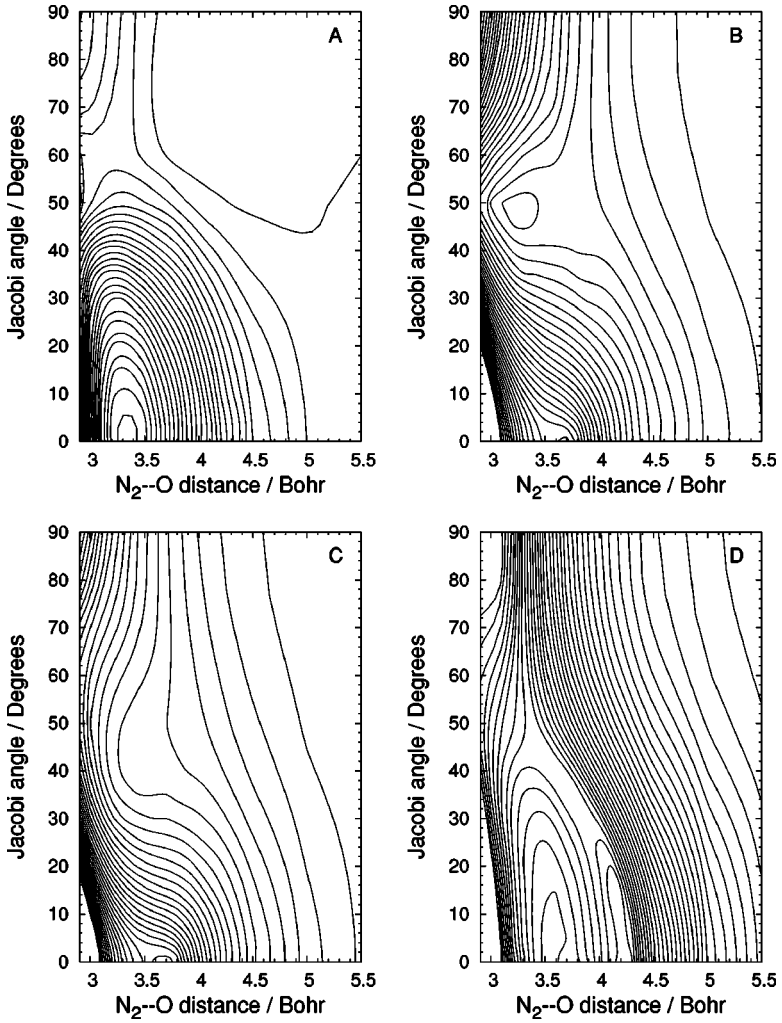

FIG. 4. Contour plots of potential energy surfaces of the four lowest singlet electronic states of N_2O. The plots are shown as a function of the N_2-O separation and the Jacobi angle with N–N separation fixed at 2.131 99 bohrs. (a) Ground state $1A'$, (b) $2A'$, (c) $1A''$, (d) $2A''$.

(AVTZ) and finally to the quadruple ζ basis minus the g-type Gaussian orbitals (AVQZ($-g$)), which are the main focus of the present work.

Figure 6 shows the effect of excitation of the bending mode on the $2A'\leftarrow 1A'$ absorption cross section. As expected excitation of the bending vibration greatly increases the absorption cross section (see Fig. 3 and discussion of the transition dipole moment surface above). This property accounts for the observed temperature behavior of the cross section,[7] which is found to increase steadily with increasing temperature.

TABLE II. Vibrational energies for low-lying states for the 2D calculation as compared with experimental measurements.

ν_1,ν_2,ν_3	ΔE (theory)[a]/cm^{-1}	ΔE (experimental)[b]/cm^{-1}
0,0,0[c]	0.00	0.00
0,1,0[d]	583.64	589.61
0,2,0[c]	1160.07	1168.13
1,0,0[c]	1269.64	1284.90

[a]$\Delta E(\text{Theory})=E(\nu_1,\nu_2,\nu_3)-E(0,0,0)$.
[b]Taken from Ref. 59.
[c]$J=0$.
[d]$J=1$ ($p=1$) since symmetry forbidden for $J=0$.

Figure 7 shows the absorption cross sections from the ground electronic state of N_2O to the two lowest $^1A''$ states ($1A''$ and $2A''$). In the vicinity of the Franck–Condon region the energies of these two electronic states lie very close to that of the $2A'$ state and the cross sections therefore form part of the first ultraviolet absorption band. It is clear from the figure that the magnitude of these cross sections is much smaller than that of the $2A'\leftarrow 1A'$ cross section (see Figs. 5 and 6). Figure 7(a) shows $1A''\leftarrow 1A'$ cross sections starting from both the lowest vibrational state and from the state with one quantum of bending vibration. We see again that the cross section for this state also increases sharply with increasing bending vibrational quantum number, but still remains very low compared to that of the $2A'\leftarrow 1A'$ cross section. The $2A''\leftarrow 1A'$ cross section displays sharp structure, characteristic of a bound-bound transition. This is in keeping with the shape of the $2A''$ ($^1\Delta$) potential energy curve [see Figs. 1, 2, and 4(d)]. The magnitude of this cross section also increases upon excitation of the bending motion. The $1A''\leftarrow 1A'$ cross section displays an unusual double hump profile. Detailed investigation shows that the origin of this line shape lies in the details of the $1A''\leftarrow 1A'$ transition dipole moment surface. In collinear geometries, in the vicinity of the Franck–Condon region, this transition dipole is

Downloaded 19 Jan 2005 to 129.128.168.123. Redistribution subject to AIP license or copyright, see http://jcp.aip.org/jcp/copyright.jsp

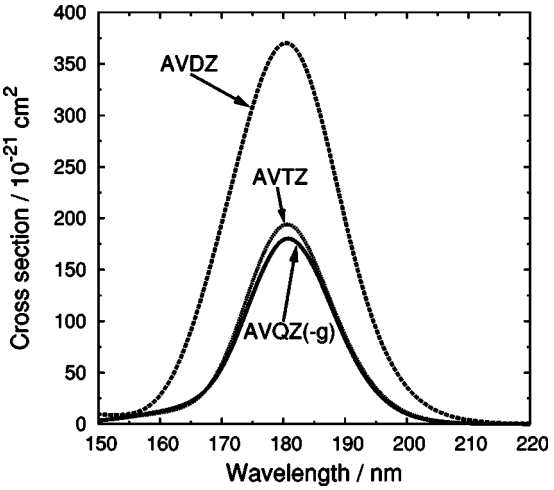

FIG. 5. $2A' \leftarrow 1A'$ cross sections using *ab initio* potential energy surfaces and transition dipole moment surfaces computed using different basis sets. AVDZ—augmented valence double ζ, AVTZ—augmented valence triple ζ, AVQZ$(-g)$—augmented valence quadruple ζ minus g-type Gaussian orbitals.

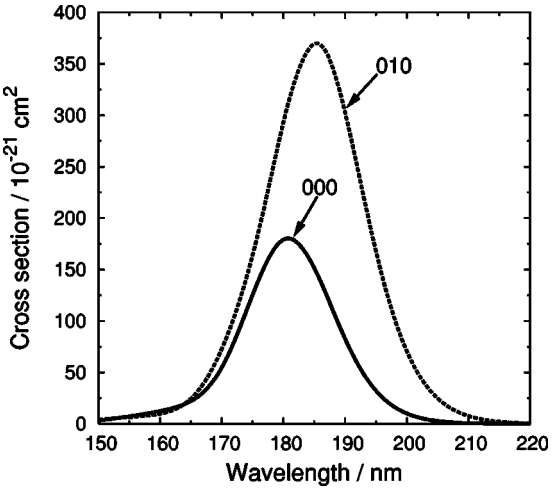

FIG. 6. $2A' \leftarrow 1A'$ cross sections starting from N_2O in it lowest vibration-rotation state and in a state with one quantum of bending vibration.

zero. At slightly bent angles, that is, in the geometry region which governs the absorption cross section, the transition dipole goes through zero as a function of the N_2-O Jacobi coordinate, close to a N_2-O separation of 3.3 bohrs. The product of the ground state vibrational wave function and the transition dipole moment, which is the initial wave packet for the time-dependent quantum dynamical propagation procedure,[45] therefore displays a double hump in this coordinate, and this in turn results in the double hump nature of the cross section as a function of photolysis energy.

The position of the peak of the main calculated absorption cross section (Fig. 6) is almost exactly at the same wavelength as that found experimentally,[33] but the width of the absorption line is considerably narrower than the experimental line shape. Our calculations have not taken account of two different line-broadening mechanisms, namely, the Renner–Teller coupling which will allow transition of the system from the $2A'$ to the $2A''$ surface and the conical intersection between the $2A'$ and the $1A'$ states (see discussion of Fig. 4 above and Ref. 27). In order to mimic the effect of these two mechanisms, both of which will result in a shortening of the lifetime of the wave packet on the excited adiabatic $2A'$ surface, we damp the autocorrelation function. This results in the broadening of the absorption line shape. An exponential and a Gaussian damping function were both investigated. It was found that the Gaussian function $[f(t) = \exp(-\alpha t^2)$; with $\alpha = 0.000\,050\,41]$ was able to provide a better fit to the important long wavelength tail of the experimental absorption line shape. Figure 8 shows the absorption line shape computed using the damped autocorrelation functions together with the experimentally measured cross section.[33] The line shape was calculated by combining the $2A' \leftarrow 1A'$ cross sections starting from both the ground vibrational state of N_2O (000) and from its first excited bending state (010). The cross sections were both weighted by their Boltzmann weighting factors corresponding to a temperature of 297 K. We see that the overall fit between the calculated and the experimental line shapes is excellent, indicating that both our computed potential energy surfaces and the transition dipole moment surfaces are accurate and reliable. The diffuse structure present in the experimentally measured line shape is absent from the calculated $2A' \leftarrow 1A'$ cross section.

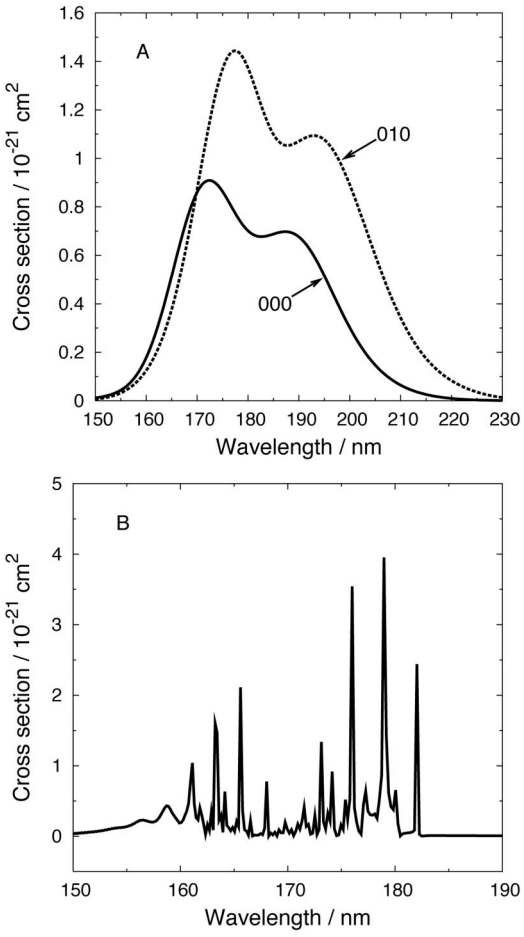

FIG. 7. N_2O $1A'' \leftarrow 1A'$ (a) and $2A'' \leftarrow 1A'$ (b) absorption cross sections.

Downloaded 19 Jan 2005 to 129.128.168.123. Redistribution subject to AIP license or copyright, see http://jcp.aip.org/jcp/copyright.jsp

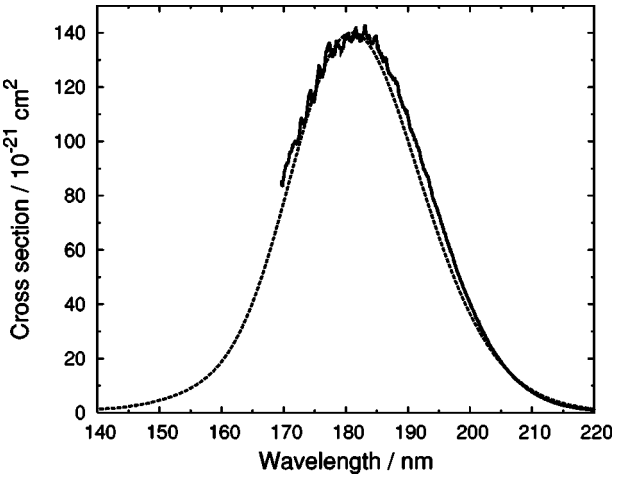

FIG. 8. N_2O absorption line shape for the $2A' \leftarrow 1A'$ absorption process, calculated from modified autocorrelation functions (dashed line), and the experimentally measured cross section (Ref. 33) (solid line). The initially computed autocorrelation functions were multiplied by a Gaussian damping function [$f(t)=\exp(-\alpha t^2)$; with $\alpha=0.000\,050\,41$]. The calculated absorption line shape is computed by taking a Boltzmann average of the cross sections starting from both the ground vibrational state of N_2O (000) and from its first excited bending state (010) using a temperature of 297 K.

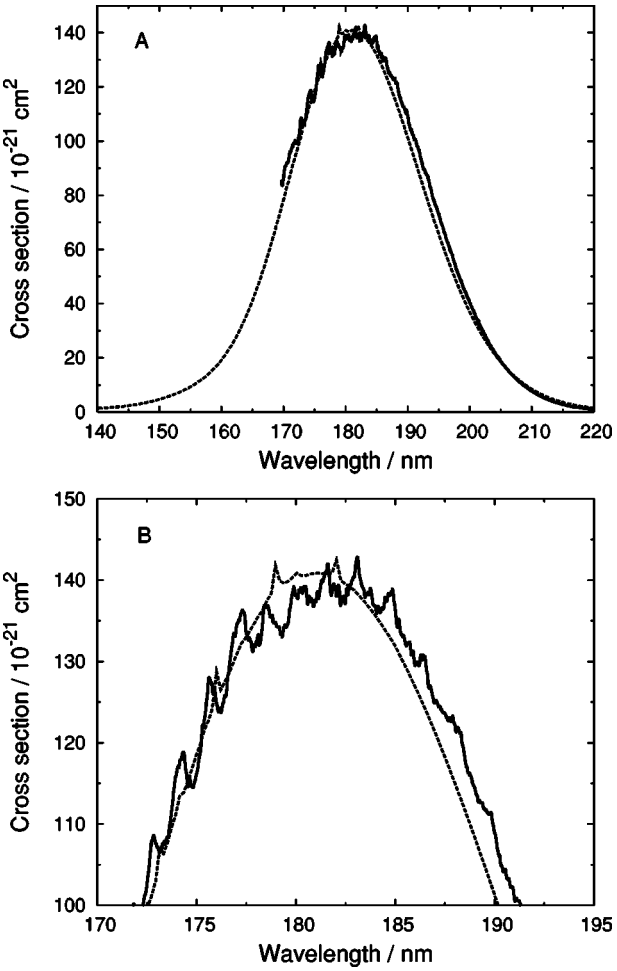

FIG. 9. Sum of line shapes (dotted line) to three lowest excited states ($1A''$, $2A'$, and $2A''$ or $^1\Sigma^-$ and $^1\Delta$) and the experimentally measured cross section (Ref. 33) (solid line). The $2A' \leftarrow 1A'$ absorption line shape was calculated using modified autocorrelation functions (see text) and all line shapes are computed as Boltzmann averages of the cross sections starting from the (000) and (010) vibrational states. (a) Entire absorption line; (b) Central region of absorption line.

Some part of the missing diffuse structure will arise from absorption to the bound $2A''$ state (see Fig. 7). Figure 9 shows the combined computed line shape for absorption to all of the three lowest excited states ($1A''$, $2A'$, and $2A''$ or $^1\Sigma^-$ and $^1\Delta$). This line shape is again calculated by using a Boltzmann average of the cross sections starting from the (000) and the (010) vibrational states of the ground electronic state. While the combined calculated line shape does show some superimposed structure, it is not as extensive as that present in the experimental line shape. Somewhat strangely the magnitude of the diffuse structure is clearly observed experimentally to increase with increasing temperature.[7] This might well be explained by an increasing contribution from absorption to the bound $2A''$ state with increasing temperature, which could possibly be brought about by the increased importance of excitation from the vibrationally excited bending state of the ground electronic state. We will examine this possibility carefully in the near future. There are at least two other possible contributors to the diffuse structure. One of these might arise from Renner-Teller coupling to the $2A''$ component of the $^1\Delta$ state. This is a bound state [see Figs. 1, 2, and 7(b)] and would lead to recurrences in the autocorrelation function, induced by flux first going from the strongly absorbing $2A'$ state to the bound $2A''$ and then recrossing, the transfers of flux being induced in both directions through the Renner-Teller coupling mechanism. Another possible contribution to the diffuse structure might come from the conical intersection between the $^1\Delta(2A')$ and the $^1\Pi(3A')$ states in collinear geometry around an N_2-O separation of 3.7 bohrs. This would provide a mechanism for crossing to the $3A'$ surface and back again. This surface again has a bound character and may create recurrences in the autocorrelation function.

During the final stages of completing this paper, another paper by Nanbu and Johnson[34] appeared (available at the time only on the web based ASAP service of Journal of Physical Chemistry) concentrating on the isotope enrichment effects arising from the photodissociation of N_2O and its isotopomers. The *ab initio* calculations of this paper were at a slightly less accurate level than those reported here (AVTZ as compared with AVQZ($-g$), see Fig. 3), but the paper reports and uses full three dimensional potential energy surfaces, which we considered would be unnecessary due to the relatively small change in N–N separation on dissociation. In their calculations Nanbu and Johnson observe very large diffuse structures which they attribute to quasibound vibrational states in the angular motion, induced by the presence of the conical intersection cone centered at around 50° and a N_2-O separation of 3.4 bohrs on the $2A'$ excited state surface.[26] Despite the fact that our potential energy surfaces appear to be very similar to theirs, we see absolutely no such structure in our calculations. We have confirmed that our computer codes can, in appropriate circumstances, produce diffuse structures through current ongoing research on the photodissociation of ozone.[58] It is possible that the potential is very sensitive to stretching of the N–N coordinate, and that it is

Downloaded 19 Jan 2005 to 129.128.168.123. Redistribution subject to AIP license or copyright, see http://jcp.aip.org/jcp/copyright.jsp

this that leads to the difference between the results of the two calculations.

Figure 10 shows the product rotational quantum state distribution arising from the $2A' \leftarrow 1A'$ photolysis of N_2O using light of wavelength 203.2 nm. The two parts of the figure correspond to N_2O being initially in its lowest rotational-vibrational state and in a state with one quantum of bending vibration. The theoretical rotational distributions can be compared to those obtained experimentally from both state-selected[12] and nonstate-selected[14,17] photodissociation at 203 nm which peak at $j_{max}=74$. We see that the calculated rotational quantum state distribution from the ground rotational-vibrational state [Fig. 10(a)] peaks exactly at the same quantum number as observed experimentally, while photolysis of an a molecule initially with one quantum of bending excitation [Fig. 10(b)] leads to a distribution which peaks at $j_{max}=75$.

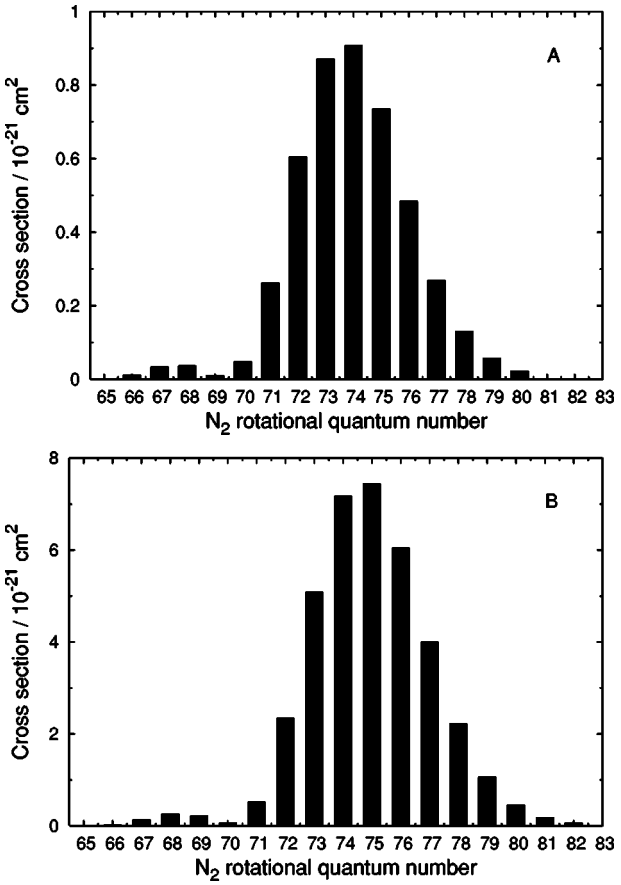

FIG. 10. Product rotational quantum state distribution resulting from the $2A' \leftarrow 1A'$ photolysis at 203 nm. N_2O initially in its (a) ground vibrational-rotational state; (b) the 010 vibrational-rotational state with one quantum of bending vibration.

IV. CONCLUSIONS

We have calculated accurate potential energy and transition dipole moment surfaces for the lowest six singlet symmetry electronic states of N_2O and have used these to study its photodissociation dynamics. The calculated surfaces clarify the complex nature of the many symmetry related and nonsymmetry related conical intersections[26] present in the system. We show that the increased accuracy of the surfaces has a marked effect on the absorption line shape (Fig. 5), with the magnitude of the cross section decreasing by over a factor of 2 as the orbital basis set is improved from AVDZ to AVQZ$(-g)$.

The computed absorption line shape is now in near quantitative agreement with the experimentally observed absorption spectrum (Fig. 8). The calculations reported here used the computed adiabatic potential energy and transition dipole moment surfaces. Because these do not allow for all the possible mechanisms which can lead to the depletion of the initial wave packet from the excited state potential energy surface to which they were first excited by absorption of a photon, we have included an empirical damping factor in the autocorrelation function to obtain the good agreement between experiment and theory displayed in Fig. 8.

The calculated rotational quantum state distribution is also in good agreement with experiment, peaking at exactly the same quantum number as the experimental observations (Fig. 10).

The main absorption in the first ultraviolet absorption band of N_2O is predominantly to the $2A'$ ($^1\Delta$) state. We have also discussed, however, the much weaker absorptions to the very close lying $1A''$ ($^1\Sigma^-$) and $2A''$ ($^1\Delta$) states (see Figs. 1 and 2). The diffuse structure present in the experimental spectrum[33] has only been partially reproduced in the calculations through the inclusion of transitions to the two lowest excited $^1A''$ states (Fig. 9). In a full three-dimensional calculation the diffuse structure arising from this excitation may be more extensive and might well reproduce the experimentally observed structure and the observed property that the magnitude of the structure increases with increasing temperature. Note particularly that the structure arising from absorption to the bound $2A''$ occurs on the short wavelength side of the absorption peak, in agreement with the experimental observations that the most marked structure occurs in this region.

Towards the final stages of completing this work a paper by Nanbu and Johnson[34] appeared in which they have performed three-dimensional quantum wavepacket calculations for the photodissociation of N_2O. Their surfaces are very similar to our own, and indeed to those published previously by two of the present authors.[26] Despite this similarity our computations do not show the same overly large diffuse structure observed in the calculations of Nanbu and Johnson. This aspect of the calculations has been discussed above and will be investigated in future work.

ACKNOWLEDGMENTS

The authors thank the EPSRC for a grant which provided the computational facilities on which these calculations were carried out. M.N.D. thanks the Public Service Department of Malaysia and the University of Malaya for a postgraduate fellowship. The authors are grateful to C.M. Western and E. Baloitcha for helpful advice.

[1] R. P. Wayne, *Chemistry of Atmospheres*, 2nd ed. (Clarendon, Oxford, 1991).

[2] *Climate Change 1994; Radiative Forcing of Climate Change and an Evaluation of the IPCC 1992 IS92 Emission Scenarios*, edited by J. T.

Downloaded 19 Jan 2005 to 129.128.168.123. Redistribution subject to AIP license or copyright, see http://jcp.aip.org/jcp/copyright.jsp

Houghton, L. G. M. Filho, and N. B. Harris (Cambridge University Press, Cambridge, 1995).
[3] M. Brouard, S. P. Duxon, P. A. Enriquez, and J. P. Simons, J. Chem. Phys. **97**, 7414 (1992).
[4] M. Brouard, H. M. Lambert, J. Short, and J. P. Simons, J. Phys. Chem. **99**, 13571 (1995).
[5] A. J. Alexander, F. J. Aoiz, M. Brouard, I. Burak, Y. Fujimura, J. Short, and J. P. Simons, Chem. Phys. Lett. **262**, 589 (1996).
[6] S. W. Leifson, Astrophys. J. **63**, 73 (1926).
[7] G. S. Selwyn and H. S. Johnston, J. Chem. Phys. **74**, 3791 (1981).
[8] W. F. Chan, G. Cooper, and C. E. Brion, Chem. Phys. **180**, 77 (1994).
[9] J. W. Rabalais, J. M. McDonald, V. Scherr, and S. P. McGlynn, Chem. Rev. (Washington, D.C.) **71**, 73 (1971).
[10] M. Zelikoff, K. Watanabe, and E. C. Y. Inn, J. Chem. Phys. **21**, 1643 (1953).
[11] K. F. Preston and R. F. Barr, J. Chem. Phys. **54**, 3347 (1971).
[12] J. M. Teule, G. C. Groenenboom, D. W. Neyer, D. W. Chandler, and M. H. M. Janssen, Chem. Phys. Lett. **320**, 177 (2000).
[13] M. Ahmed, E. R. Wouters, D. S. Peterka, O. S. Vasyutinskii, and A. G. Suits, Faraday Discuss. **113**, 425 (1999).
[14] D. W. Neyer, A. J. R. Heck, and D. W. Chandler, J. Chem. Phys. **110**, 3411 (1999).
[15] D. W. Neyer, A. J. R. Heck, D. W. Chandler, J. M. Teule, and M. H. M. Janssen, J. Phys. Chem. A **103**, 10388 (1999).
[16] T. Suzuki, H. Katayanagi, Y. Mo, and K. Tonokura, Chem. Phys. Lett. **256**, 90 (1996).
[17] T. F. Hanisco and A. C. Kummel, J. Phys. Chem. **97**, 7242 (1993).
[18] L. L. Springsteen, S. Satyapal, Y. Matsumi, L. M. Dobeck, and P. L. Houston, J. Phys. Chem. **97**, 7239 (1993).
[19] P. Felder, B.-M. Haas, and J. R. Huber, Chem. Phys. Lett. **186**, 177 (1991).
[20] N. Shafer, K. Tonokura, Y. Matsumi, S. Tasaki, and M. Kawasaki, J. Chem. Phys. **95**, 6218 (1991).
[21] M. Brouard, P. O'Keeffe, M. D. Joseph, and D. Minayev, Phys. Rev. Lett. **86**, 2249 (2001).
[22] M. Brouard, A. P. Clark, C. Vallance, and O. S. Vasyutinskii, J. Chem. Phys. **86**, 2249 (2001).
[23] M. S. Johnson, G. D. Billing, A. Gruodis, and M. H. M. Janssen, J. Phys. Chem. A **105**, 8672 (2001).
[24] M. K. Prakash, J. D. Weibel, and R. A. Marcus (unpublished).
[25] D. G. Hopper, J. Chem. Phys. **80**, 4290 (1984).
[26] A. Brown, P. Jimeno, and G. Balint-Kurti, J. Phys. Chem. A **103**, 11089 (1999).
[27] A. Brown and G. G. Balint-Kurti, unpublished wave packet calculations using the surfaces of Ref. 26 (2000).
[28] A. T. Wong and G. B. Bacskay, Chem. Phys. Lett. **207**, 360 (1993).
[29] C. Frind, L. Asbrink, and F. Lindholm, Chem. Phys. **27**, 169 (1978).
[30] N. W. Winter, Chem. Phys. Lett. **33**, 300 (1975).
[31] A. Chutjian and G. A. Segal, J. Chem. Phys. **57**, 3069 (1972).
[32] S. D. Peyerimhoff and R. J. Buenker, J. Chem. Phys. **49**, 2473 (1968).
[33] K. Yoshino, D. E. Freeman, and W. H. Parkinson, Planet. Space Sci. **32**, 1219 (1984); Spectral data can be downloaded from Harvard-Smithsonian Center for Astrophysics Molecular Data base; web address: http://cfa-www.harvard.edu/amdata/ampdata/cfamols.html
[34] S. Nanbu and M. S. Johnson, J. Phys. Chem. A **108**, 8905 (2004).
[35] H.-J. Werner and P. J. Knowles, MOLPRO, a package of *ab initio* programs version 2002.1, contributions from R. D. Amos, A. Bernhardsson, A. Berning, P. Celani, D. L. Cooper, M. J. O. Deegan, A. J. Dobbyn, F. Eckert, C. Hampel, G. Hetzer, P. J. Knowles, T. Korona, R. Lindh, A. W. Lloyd, S. J. McNicholas, F. R. Manby, W. Meyer, M. E. Mura, A. Nicklass, P. Palmieri, R. Pitzer, G. Rauhut, M. Schtz, U. Schumann, H. Stoll, A. J. Stone, R. Tarroni, T. Thorsteinsson, and H.-J. Werner.
[36] H.-J. Werner and P. J. Knowles, J. Chem. Phys. **82**, 5053 (1985).
[37] P. J. Knowles and H.-J. Werner, Chem. Phys. Lett. **115**, 259 (1985).
[38] H.-J. Werner and P. J. Knowles, J. Chem. Phys. **89**, 5803 (1988).
[39] P. J. Knowles and H.-J. Werner, Chem. Phys. Lett. **145**, 514 (1988).
[40] T. H. Dunning, Jr., J. Chem. Phys. **90**, 1007 (1989).
[41] R. A. Kendall, T. H. Dunning, Jr., and R. J. Harrison, J. Chem. Phys. **96**, 6796 (1992)
[42] G. G. Balint-Kurti, L. Füsti-Molnár, and A. Brown, Phys. Chem. Chem. Phys. **3**, 702 (2001).
[43] W. H. Press, S. A. Teukolsky, W. T. Vetterling, and B. P. Flannery, *Numerical Recipes in Fortran 77: The Art of Scientific Computing*, 2nd ed. (Cambridge University Press, Cambridge, 1996).
[44] G. G. Balint-Kurti, *Time Dependent Quantum Approaches to Chemical Reactivity*, in Lecture Notes in Chemistry Vol. 75, edited by A. Lagan and A. Riganelli (Springer Berlin, 2000), p. 74.
[45] G. G. Balint-Kurti, Adv. Chem. Phys. **128**, 249 (2003).
[46] I. F. Kidd and G. G. Balint-Kurti, J. Chem. Phys. **82**, 93 (1985).
[47] G. G. Balint-Kurti, R. N. Dixon, and C. C. Marston, Int. Rev. Phys. Chem. **11**, 317 (1992).
[48] J. C. Light, I. P. Hamilton, and V. J. Lill, J. Chem. Phys. **82**, 1400 (1985).
[49] A. R. Offer and G. G. Balint-Kurti, J. Chem. Phys. **101**, 10416 (1994).
[50] C. Leforestier, J. Chem. Phys. **94**, 6388 (1991).
[51] G. Corey and D. Lemoine, J. Chem. Phys. **97**, 4115 (1992).
[52] K. Ahmed, G. G. Balint-Kurti, and C. M. Western, J. Chem. Phys. **121**, 10041 (2004).
[53] G. G. Balint-Kurti and A. Brown, in *Theory of Chemical Reaction Dynamics*, edited by A. Lagana and G. Lendvay (Kluwer Academic, Dordrecht, 2004), p. 149.
[54] Á. Vibók and G. G. Balint-Kurti, J. Chem. Phys. **96**, 7615 (1992).
[55] Á. Vibók and G. G. Balint-Kurti, J. Phys. Chem. **96**, 8712 (1992).
[56] G. G. Balint-Kurti and Á. Vibók, in: *Numerical Grid Methods and their Application to Schrdinger's Equation*, NATO Advanced Studies Institute series, Series C: Mathematical and Physical Sciences, edited by C. Cerjan (Kluwer Academic Publishers, Dordrecht, 1993), Vol. 412, p. 195.
[57] See EPAPS Document No. E-JCPSA6-122-303502 for the *ab initio* potential energy surfaces for the $\tilde{X}\ ^1A'$, $2\ ^1A'$, $1\ ^1A''$, and $2\ ^1A''$ electronic states and the *ab initio* electronic transiton dipole moment surfaces for the ground state to the other states. A direct link to this document may be found in the online article's HTML reference section. The document may also be reached via the EPAPS homepage (http://www.aip.org/pubservs/epaps.html) or from ftp.aip.org in the directory /epaps/. See the EPAPS homepage for more information.
[58] E. Baloitcha, G. G. Balint-Kurti, and A. Brown (unpublished).
[59] R. A. Toth, Appl. Opt. **30**, 5289 (1991).

Downloaded 19 Jan 2005 to 129.128.168.123. Redistribution subject to AIP license or copyright, see http://jcp.aip.org/jcp/copyright.jsp